Journal of Cerebral Blood Flow and Metabolism
21:1342–1353 © 2001 The International Society for Cerebral Blood Flow and Metabolism
Published by Lippincott Williams & Wilkins, Inc., Philadelphia

Positron Emission Tomography Quantification of [^{11}C]-DASB Binding to the Human Serotonin Transporter: Modeling Strategies

Nathalie Ginovart, Alan A. Wilson, Jeffrey H. Meyer, Doug Hussey, and Sylvain Houle

PET Center, Center for Addiction and Mental Health, and University of Toronto, Toronto, Ontario, Canada

Summary: [^{11}C]-DASB, namely [^{11}C]-3-amino-4-(2-dimethylaminomethyl-phenylsulfanyl)-benzonitrile, is a new highly selective radioligand for the *in vivo* visualization of the serotonin transporter (SERT) using positron emission tomography (PET). The current study evaluates different kinetic modeling strategies for quantification of [^{11}C]-DASB binding in five healthy humans. Kinetic analyses of tissue data were performed with a one-tissue (1CM) and a two-tissue (2CM) compartment model. Time-activity curves were well described by a 1CM for all regions. A 2CM model with four parameters failed to converge reliably. Reliable fits of the data were obtained only if no more than three parameters were allowed to vary. However, even then, the rate constants k_3 and k_4 were estimated with poor precision. Only the ratio k_3/k_4 was stable. Goodness of fit was not improved by using a 2CM as compared with a 1CM. The minimal study duration required to obtain stable k_3/k_4 estimates was 80 minutes. For routine use of [^{11}C]-DASB, several simplified methods using the cerebellum as a reference region to estimate nonspecific binding were also evaluated. The transient equilibrium, the linear graphical analysis, the ratio of target to reference region, and the simplified reference tissue methods all gave binding potential values consistent with those obtained with the 2CM. The suitability of [^{11}C]-DASB for research on the SERT using PET is thus supported by the observations that tissue data can be described using a kinetic analysis and that simplified quantitative methods, using the cerebellum as reference, provide reliable estimates of SERT binding parameters. **Key Words:** [^{11}C]-DASB—Human—Modeling—PET—Serotonin transporter.

Alterations in the serotonin transporter (SERT) have been described in several neuropsychiatric conditions. Postmortem studies reported decreased SERT densities in cortical and subcortical regions of Parkinsonian subjects (Cash et al., 1985), depressed patients (Crow et al., 1984), and suicide victims (Stanley et al., 1982). In addition to its association with pathophysiologic processes, the SERT is the primary target of the widely prescribed specific serotonin reuptake inhibitors (SSRIs). Given the wide use of these drugs in the treatment of depression, there is a strong incentive to explore their biochemical effects directly in patients. In the study of the mode of action of both existing and new antidepressant drugs keen insight thus would be gained with the ability to measure their occupancy, their pharmacokinetics, and their effect on regulation of the SERT *in vivo*. Such an approach can be performed in the living human brain using positron emission tomography (PET) and a suitable radioligand for the SERT.

Several radioligands have been developed as PET markers for the SERT. These radioligands differ with respect to their affinities and specificities for the SERT, their specific to nonspecific binding ratios, and their brain kinetics. Successful conversion of paroxetine, a ligand of choice for labeling the SERT *in vitro*, into a PET imaging agent has not been accomplished despite its high potency for uptake inhibition (Suehiro et al., 1991). Other SSRIs drugs with high affinity for the SERT, such as sertraline, citalopram, or fluoxetine, have been labeled with ^{11}C but also displayed low specific-to-nonspecific binding ratios *in vivo* (Hashimoto et al., 1987; Lasne et al., 1989; Shiue et al., 1995; Hume et al., 1992). McN-5652 is another potent blocker of serotonin uptake although it displays a moderate selectivity toward the dopamine and norepinephrine transporters (Maryanoff et al., 1990). [^{11}C](+)-McN-5652 has been described as a promising PET radiotracer for the SERT in the baboon brain, with a modest specific-to-nonspecific ratio (Szabo et al., 1995). However, the low specific-to-nonspecific

Received April 17, 2001; final revision received July 20, 2001; accepted July 23, 2001.

Supported by grants from Eli Lilly and from the Medical Research Council of Canada (Grant # MA-14711).

Address correspondence and reprint requests to Nathalie Ginovart, PET Center, CAMH, 250 College Street, Toronto, Ontario, M5T 1R8, Canada.

binding ratios observed with [^{11}C](+)-McN-5652 in humans, together with the extended acquisition time required to obtain stable estimates of SERT density indices, limit its application as a PET imaging agent *in vivo* (Parsey et al., 2000). *In vivo* PET imaging of SERT thus would clearly benefit from the development of a radiotracer with high selectivity for the SERT and high levels of signal-to-noise ratios.

A new class of potent SSRIs recently has been described, namely *N*-methyl-2-(arylthio)benzylamines, which possess a high affinity and selectivity for the SERT. Two derivatives of this class of compounds, IDAM and ADAM, have been described to display subnanomolar affinities for the SERT and a high selectivity over the dopamine and noradrenaline transporters both *in vitro* and *in vivo* in rats (Kung et al., 1999; Choi et al., 2000). Both derivatives have been labeled with ^{123}I and were described as suitable radioligands for *in vivo* visualization of the SERT using single photon emission computerized tomography (SPECT) in primates (Acton et al., 1999; Oya et al., 1999, 2000). The authors have recently synthesized and radiolabeled with ^{11}C a series of *N*-methyl-2-(arylthio)benzylamines analogues for PET visualization of the SERT (Wilson and Houle, 1999; Wilson et al., 2000*a*). Four of these compounds displayed nanomolar or subnanomolar affinity for the SERT, and a greater than 1,000-fold affinity for the cloned human SERT over the dopamine transporter and the norepinephrine transporter in *in vitro* binding essays (Wilson et al., 2000*a*). *Ex vivo* studies of the brain pharmacokinetics of one of these analogues, namely [^{11}C]-DASB ([^{11}C]-3-amino-4-(2-dimethylaminomethyl-phenylsulfanyl)-benzonitrile), have given promising results in rats and showed that [^{11}C]DASB binding in SERT-rich brain regions was both saturable and specific for the SERT (Wilson et al., 2000*a*). Preliminary studies in humans showed that the regional distribution of [^{11}C]-DASB uptake was concordant with the known densities of SERT sites in the brain (Houle et al., 2000). However, further validation for the use of this radioligand in humans is required.

The aim of this study was to evaluate the prospect of using [^{11}C]-DASB for quantification of SERT populations in the human brain. Regional brain uptake curves of [^{11}C]-DASB were quantified using kinetic modeling analyses based on either one- or two-tissue compartments and involving two to four rate constants. In addition, simplified methods were evaluated to determine the most appropriate method for quantification of [^{11}C]-DASB binding in routine clinical research.

MATERIALS AND METHODS

Subjects

This study was approved by the Human Subjects Review Committee of the University of Toronto. Five healthy volunteer subjects (3 men and 2 women, aged 25 to 50 years) were recruited and provided their informed consent before participation. Subjects were screened for history of psychiatric and medical illnesses. None of the subjects was taking any drugs.

Radiochemistry

[^{11}C]-DASB was synthesized as described previously (Wilson et al., 2000*a,b*). Briefly, [^{11}C]-CH_3I was trapped in a high performance liquid chromatography (HPLC) sample loop coated with a solution of the N-normethyl precursor (1 mg) in dimethylformamide (80 μL). After 5 minutes at ambient temperature, the contents of the sample loop were injected onto a reverse-phase HPLC column, and the fraction containing product collected, evaporated to dryness, formulated in saline, and filtered through a 0.2 μm filter. Radiochemical purities were greater than 98%.

Positron emission tomography system

Studies were performed on an 8-ring brain PET camera system Scanditronix GEMS 2048–15B (Scanditronix Medical, General Electric, Uppsala, Sweden) that measured radioactivity in 15 brain sections with a thickness of 6.5 mm each (Litton et al., 1990). The intrinsic inplane resolution of the reconstructed images is 4.5 mm full width at half maximum. Transmission scans were acquired with rotating ^{68}Ge sources and were used to correct the emission scans for the attenuation of 511 keV photons through tissue and head support. Images were reconstructed using the transmission scan data for attenuation correction and a Hanning 5-mm filter.

Positron emission tomography studies

A thermoplastic mask was made for each subject and was used with a head fixation system during the PET measurements. Cannulae were inserted in the radial artery for blood sampling and in the controlateral arm antecubital vein for radioligand injection. A saline solution of 10.2 mCi (SD = 1.2 mCi) [^{11}C]-DASB at a specific radioactivity of 1000 Ci/mmol (SD = 145 Ci/mmol) was injected intravenously as a bolus immediately flushed with 10 mL saline. Radioactivity in brain was measured in a series of sequential frames of increasing duration (from 1 to 5 minutes). In 3 subjects, the total time for measurement of radioactivity in brain was 90 minutes; it was extended to 120 minutes in the remaining 2 subjects.

An automatic blood sampling system was used to measure radioactivity in arterial blood during the first 20 minutes of the experiment. At the same time and thereafter, manual blood samples were drawn at 5, 10, 15, 20, 30, 45, 60, and 80 minutes after radiotracer injection. An additional blood sample was withdrawn at 110 minutes in the 2 subjects for which PET scanning time was extended to 120 minutes. An aliquot of each blood sample was taken to measure radioactivity concentration in total blood. The remainder of blood was centrifuged (1500 *g*, 5 minutes) and a plasma aliquot counted together with the total blood sample using a Cobra II gamma counter (Packard Instrument Company, Downers Grove, IL, U.S.A.) crosscalibrated with the PET system. Blood-to-plasma ratios determined from the manual samples were used to correct the blood radioactivity time-activity curve measured by automatic sampling and to generate the plasma radioactivity curve. The remaining volume of each manual plasma sample (3 mL) was used to determine unchanged radioligand and its metabolites in plasma. The fraction of unchanged ligand in plasma was fitted to a sum of two exponential functions. A metabolite-corrected plasma curve was generated by the product of the two curves. The corrected plasma curve was then fitted to a sum of three exponential functions (with the ascending part of the curve linearly interpolated between measured values), and the resulting fitted

curve was used as input function ($C_P(t)$, nCi/mL) for the kinetic and graphical analyses.

Determination of ligand metabolism in plasma

In each experiment, the fraction of plasma radioactivity representing unchanged [^{11}C]-DASB was determined by a combination of solid phase extraction and HPLC. Plasma samples (3 mL) were applied to a solid-phase extraction cartridge (OASIS 6 cc; Waters, Milford, MA, U.S.A.), which was preconditioned with 5 mL each of tetrahydrofuran (THF), ethanol (EtOH), and water. The cartridge then was eluted by partial vacuum and washed successively with 5 mL 5% methanol (MeOH) in water, 5 mL 22% acetonitrile (CH_3CN) in water containing 0.1 N ammonium formate, and 1.5 mL THF. Each of the fractions, the cartridge, the whole blood and plasma samples were counted for radioactivity. The THF fraction was evaporated in a stream of nitrogen to near dryness, taken up in 250 μL HPLC buffer, and analyzed by HPLC for metabolites. HPLC analysis was performed using a Novapak C18 column (300 × 7.5 mm; Waters) using 40:60 CH_3CN/H_2O + 0.1 N ammonium formate at 5 mL/min with inline UV (254 nmol/L) and radioactivity detectors (LB507A; Berthold Technologies, Bad Wildbad, Germany). Binding of [^{11}C]-DASB to human plasma proteins was performed using an ultrafiltration technique described previously (Price et al., 1993).

Regions of interest

Each subject had a brain magnetic resonance imaging (MRI) examination. T_1-weighted and proton density images were obtained on a Signa 1.5 T MRI scanner (General Electric Medical System, Milwaukee, WI, U.S.A.). Both T_1-weighted and proton density images were acquired with spin-echo pulse sequences. Each subject's MRI scan was co-registered to the PET scan using Rview8/mpr realignment software (Studholme et al., 1997).

Regions of interest (ROIs) for the striatum, thalamus, hypothalamus, occipital cortex, frontal cortex, and cerebellum were drawn with reference to the co-registered MRI. Each ROI was drawn in two adjacent sections, in both hemispheres, and data from the same ROI were pooled to obtain the average radioactivity concentration in the volume of interest. Regional radioactivity was determined for each frame, corrected for decay, and plotted versus time.

Data analysis

Kinetic analysis. Kinetic analysis of tissue data was performed with a 1CM and a 2CM. The 2CM (Fig. 1A) includes: the radioactivity concentration of unchanged radioligand in plasma (C_P), the concentration of radioligand free and nonspecifically bound in tissue (C_{NS+F}), and the concentration of radioligand specifically bound to receptor sites (C_B). The rate constants K_1 (mL g^{-1} min^{-1}) and k_2 (min^{-1}) describe the influx and efflux rates, respectively, for radioligand diffusion through the blood–brain barrier. The rate constants k_3 and k_4 describe the radioligand transfer between the nondisplaceable compartment (that is, C_{NS+F}) and the specific binding compartment (C_B). Model equations for the 2CM analysis of radiotracer binding to receptors are given by

$$dC_{NS+F}(t)/dt = K_1C_P(t) - (k_2 + k_3)C_{NS+F}(t) + k_4C_B(t) \quad (1)$$

$$dC_B(t)/dt = k_3C_{NS+F}(t) - k_4C_B(t) \quad (2)$$

The rate constant k_3 (min^{-1}) is the product of the bimolecular association rate constant k_{on} and the concentration of available receptors (B_{max} − B), with B << B_{max} because experiments were performed at tracer dose and high specific radioactivity. At such conditions, $k_3 = (k_{on}\ B_{max})$. k_4 (min^{-1}) is the unimolecular receptor dissociation rate constant k_{off}. After replacement of k_3 and k_4, Eq. 2 can be written as

$$dC_B(t)/dt = (k_{on}B_{max})C_{NS+F}(t) - k_{off}C_B(t) \quad (3)$$

At equilibrium (that is, $dC_B(t)/dt = 0$), the ratio k_3/k_4 can be defined as the ratio B_{max} over K_D, which is referred to as the binding potential (BP) (Mintun et al., 1984):

$$BP = k_3/k_4 = B_{max}/K_D \quad (4)$$

with $K_D = (k_{off} / k_{on})$. The BP calculated from the ratio k_3/k_4 obtained using the 2CM analysis is referred as BP_{kin}.

The concept of distribution volume (DV) (mL g^{-1}) is also frequently used in tracer kinetics to estimate binding site density. The total DV (DV_T) has the advantage to be a more stable parameter than the individual kinetic parameters determined from compartmental analysis (Koeppe et al., 1991; Carson et al., 1993). The DV_T of a radioligand in a tissue is the volume of tissue in which the radioligand would have to distribute to reach a concentration equal to that in plasma. It is defined as the sum of the DV in the free and nonspecifically bound compartment (DV_{NS+F}) and the DV in the specifically bound compartment (DV_B). DV_{NS+F} and DV_B can be expressed in terms of the kinetic rate parameters as follows:

$$DV_{NS+F} = K_1/k_2 \quad (5)$$

$$DV_B = (K_1/k_2)(k_3/k_4) \quad (6)$$

By combining Eqs. 5 and 6:

$$DV_T = (K_1/k_2)(1 + k_3/k_4) = (K_1/k_2)(1 + B_{max}/K_D) \quad (7)$$

A simplification of the 2CM into a 1CM can be made by assuming that the concentrations C_{NS+F} and C_B equilibrate rapidly and are combined in one single compartment noted C_T (Fig. 1B). The total distribution volume for the 1CM is noted as DV′ and is given by

$$DV' = K_1/k_2' \quad (8)$$

$$k_2' = k_2/(1 + k_3/k_4) \quad (9)$$

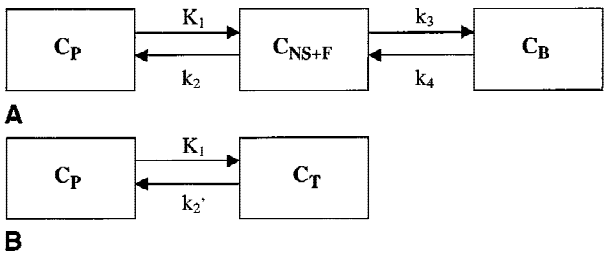

FIG. 1. Two-tissue **(A)** and one-tissue **(B)** compartment models used for kinetic analysis of [^{11}C]-DASB binding.

Nonlinear least square fitting. Nonlinear least squares fitting (NLSF) analyses using the Marquardt algorithm (Marquardt, 1963) and based on the 1CM and 2CM were applied to the time-activity curves for regional [^{11}C]-DASB uptake. Cerebral blood volume was fixed at 5% for all ROIs (Leenders et al., 1990).

Different model configurations were used for analysis of [^{11}C]-DASB kinetics (Table 1). Method A was based on the 1CM, and NLSF analyses were performed to estimate K_1, k_2', and DV′. Method B was based on the 2CM, and NLSF analyses were performed to estimate the 4 rate constants K_1, k_2, k_3, k_4. To improve the stability of the fits, four other fitting strategies were tested. All four were based on the 2CM. In Method C, the

TABLE 1. *Fitting strategies used for kinetic modeling of [^{11}C]-DASB*

Method	Number of tissue compartments	Constraints
A	1	None
B	2	None
C	2	K_1/k_2 fixed
D	2	K_1/k_2 coupled
E	2	k_4 coupled
F	2	K_1/k_2 and k_4 coupled

ratio K_1/k_2 in target ROIs was fixed to the DV′ value estimated in the cerebellum using the 1CM, under the assumption that radioactivity in cerebellum represent free and nonspecifically bound radiotracer and that DV_{NS+F} is similar between regions. Three rate constants—K_1, k_3, and k_4 (with $k_2 = K_1/DV_{NS+F}$)—were estimated. Methods D, E, and F used several combinations of parameter coupling as previously described by Buck et al. (1996). In these latter methods, it was assumed that certain parameters such as the ratio K_1/k_2 and k_4 were similar between regions. Nonlinear least squares fitting analyses were accordingly performed by fitting simultaneously data from all regions and guided by the constraint of finding parameter values common to all regions. Nonlinear least squares fitting analyses were performed using the dedicated software PMOD (Burger and Buck, 1997; Mikolajczyk et al., 1998).

Statistics. Several statistical methods were used to compare the two models. Goodness of fit was evaluated using the Akaike information criterion (AIC) (Akaike, 1974), the Schwartz criterion (SC) (Schwartz, 1978), and F test statistics. Higher AIC and SC values were indicative of a better fit. Statistical significance using the F test was assumed for $P \geq 0.05$.

The standard error of the parameters was given by the diagonal of the covariance matrix (Carson, 1986), expressed as percentage of the parameter value (coefficient of variation, %COV), and used to assess the parameter identifiability by the NLSF procedure. Calculation of %COV was possible only for fitted parameters. For derived parameters such as k_3/k_4, the SD of the mean (n = 5 subjects) was calculated, expressed as percentage of the mean derived parameter value, and used as an indication of the stability of the parameter estimate (%VAR = SD/mean × 100).

Effect of study duration on parameter estimates

The effect of study duration on parameter stability was estimated by shortening the fitting interval. Study durations ranging from 40 to 90 minutes after [^{11}C]-DASB injection were evaluated. The identifiability of DV′ (Method A) and k_3/k_4 (Method C) was evaluated in each region. For each region and duration, each parameter was expressed as the percentage of the value obtained when 90 minutes of scanning data was considered. The SD on the mean of each parameter value was used as an indication of the stability of the parameter estimate. In addition, in the 2 subjects for whom PET data acquisition time was extended to 120 minutes, regional time-activity curves also were fitted for 100, 110, and 120 minutes, and the outcome measures obtained at these extended times were compared to the 90-minute value.

Simplified method analyses

Simplified methods were applied to determine the stability and reliability of BP. Evaluation of the various methods to determine [^{11}C]-DASB BP was based on both the comparison with BP values obtained from the kinetic modeling approach and the degree of intersubject variability (%VAR) of the parameter. Several simplified approaches were evaluated.

Linear graphical analysis: BP_{Logan}. The graphic approach described by Logan et al. (1990) for the analysis of reversible radioligand binding was applied for the quantification of [^{11}C]-DASB. A plasma input function corrected for the presence of labeled metabolites ($C_P(t)$) was used. The ratio $\int_0^t ROI(t')dt'/ROI(t)$ was plotted versus $\int_0^t C_P(t')dt'/ROI(t)$, with ROI(t) describing radioactivity in a defined ROI as a function of time. The DV_T of the radioligand in that ROI was determined from the linear portion of the plot obtained. The ratio of the DV_T in a ROI to that obtained in cerebellum, a reference region containing negligible densities of SERT, is related to the SERT binding site parameter by

$$BP_{Logan} = (DV_{ROI}/DV_{ref}) - 1 \quad (10)$$

Simplified reference tissue model: BP_{SRTM}. According to this approach, the time-activity curves for a region devoid of specific binding sites, C_{NS+F} (t), is used as an indirect input function, $C_P(t)$. For [^{11}C]-DASB, the cerebellum was used as the reference region, assuming that no SERT sites are present in this region. The major assumptions of this approach are that the exchange rates between the nondisplaceable and specific compartments are so fast that they are combined in a single compartment, and that the level of nondisplaceable binding in the reference and the target regions is similar (Lammertsma and Hume, 1996). An expression including BP can be derived that relates radioligand concentration in a target region to the radioligand concentration in the reference region. From the time-activity curves measured in the reference and in the target regions, best estimates of BP can be obtained using NLSF analysis. The BP calculated with this approach is referred to as BP_{SRTM}.

Ratio analysis: BP_{ratio}. The time curve for specific radioligand binding was defined as the radioactivity concentration in a ROI subtracted with that in the cerebellum: $C_B(t) = C_{ROI}(t) - C_{CEREB}(t)$. Radioactivity in the cerebellum thus was used as an estimate for C_{NS+F}. The time curves for C_B and C_{NS+F} were integrated at late times—that is, from t_1 = 55 minutes to t_2 = 90 minutes. The BP_{ratio} was calculated according to the following equation:

$$BP_{ratio} = \int_{t_1}^{t_2} C_B(t)dt \Big/ \int_{t_1}^{t_2} C_{NS+F}(t)dt \quad (11)$$

Transient equilibrium analysis: BP_{Eq}. Time for transient equilibrium was defined as the moment when $C_B(t)$ peaked—that is, $dC_B/dt = 0$ (Farde et al., 1989). A set of three exponential functions was fitted to the time curves for $C_B(t)$ and $C_{NS+F}(t)$, and the peak for $C_B(t)$ was defined on the fitted curve. The ratio between C_B and C_{NS+F} obtained at transient equilibrium is equal to k_3/k_4 and is referred here as BP_{Eq}.

Simulation study

A simulation study was performed to estimate the error induced by regional changes in radioligand delivery on BP values calculated using both the ratio method and the SRTM. Changes in radioligand delivery, such as caused by changes in cerebral blood flow (CBF), were simulated by changing the K_1 value by ±30% (in 10% increments) around the K_1 value obtained from the 2CM. Tissue time-activity curves obtained in the striatum of one specific subject (90 minutes of data acquisition) were fitted according to Method F. The kinetic parameters derived from the fitted curve were: $K_1 = 0.87$ mL g^{-1} min^{-1}; $K_1/k_2 =$

13.63 mL g^{-1}, $k_3 = 1.27$ min^{-1}, $k_4 = 0.72$ min^{-1}. Simulated tissue time-activity curves were generated with the K_1/k_2 and the k_4 values fixed to the values derived from Method F, with K_1 values ranging from 0.61 to 1.13 mL g^{-1} min^{-1} and with k_3 values ranging from 0.36 to 2.16 min^{-1}, which corresponded to k_3/k_4 values ranging from 0.5 to 3. A cerebellar time-activity curve also was generated according to the 1CM with $K_1 = 0.76$ mL g^{-1} min^{-1} and $k_2' = 0.056$ min^{-1}. BP_{ratio} and BP_{SRTM} then were calculated using those simulated time-activity curves. For each assumed k_3/k_4 value, BP_{ratio} and BP_{SRTM} were compared to the corresponding BP value obtained when using the original fitted time-activity curves—that is, $K_1 = 0.87$ mL g^{-1} min^{-1}.

RESULTS

Plasma analysis

The HPLC analysis of the THF fractions showed only the presence of unmetabolized [^{11}C]-DASB in all human subjects analyzed at every time points examined in all subjects. Furthermore, previous experiments in which whole human blood was spiked with [^{11}C]-DASB demonstrated that more than 97% of the radioactivity was eluted in the THF fraction (data not shown). These data indicate that measuring radioactivity in the successive fractions eluted from the solid-phase extraction cartridge is sufficient to determine the fraction of radioactive metabolites in human plasma. HPLC analysis thus is not required for future analysis of [^{11}C]-DASB metabolism.

The fraction of unmetabolized [^{11}C]-DASB in plasma decreased throughout the time-course of the study and was approximately 40% ± 7% at 30 minutes and 17% ± 3.5% at 80 minutes (Fig. 2A). All metabolites were more polar than the parent compound and thus unlikely to pass the blood–brain barrier. The free fraction of [^{11}C]-DASB in plasma was determined to be 11.0% ± 1.2%. Figure 2B shows a representative curve for unchanged radioactivity in plasma, which was used as input function in the NLSF and graphical analyses.

Kinetic analyses

Characteristic time-activity curves obtained after intravenous injection of [^{11}C]-DASB in one subject are shown in Fig. 3. The highest radioactivity concentration was observed in hypothalamus, intermediate levels were observed in thalamus and striatum, and modest to low levels of radioactivity were observed in cortical regions and cerebellum, respectively. Radioactivity levels peaked at approximately 20 minutes postinjection in the cerebellum and cortical regions, whereas it peaked later in both the striatum and thalamus (between 30 and 40 minutes) and in the hypothalamus (between 50 and 60 minutes).

1CM configuration. Results obtained from NLSF analyses using Method A are presented in Table 2. Tissue time-activity curves were well-described by a 1CM and convergence was achieved for all regions. The rate constant K_1 was high and ranged from 0.62 mL g^{-1} min^{-1} in the hypothalamus to 0.79 mL g^{-1} min^{-1} in the thalamus. K_1 values were well identified in all regions with %COV close to 2%. The rate constant k_2' showed a larger variation between regions with values raging from 0.013 min^{-1} in a region rich in SERT sites such as the hypothalamus to 0.053 min^{-1} in cerebellum, a region devoid of SERT. This parameter was also well identified in all regions with %COVs inferior to 5%. The rank order for DV′ values estimated with the 1CM was: hypothalamus > thalamus > striatum > occipital cortex > frontal cortex > cerebellum.

2CM configuration. Results obtained using the 2CM configuration are presented in Table 3. Only data obtained with Methods C, D, and F are presented. Indeed, Methods B and E both failed to reach convergence in all regions and all subjects. Extension of PET data acquisition time from 90 to 120 minutes did not solve problems with model convergence in the 2 subjects tested. In all subjects, reliable fits of the data were obtained only if no more than three parameters were allowed to vary. Constraining the 2CM fitting procedure removed the convergence difficulties and resulted in adequate fits of the data. In Method C, fixing the free plus nonspecific DV in

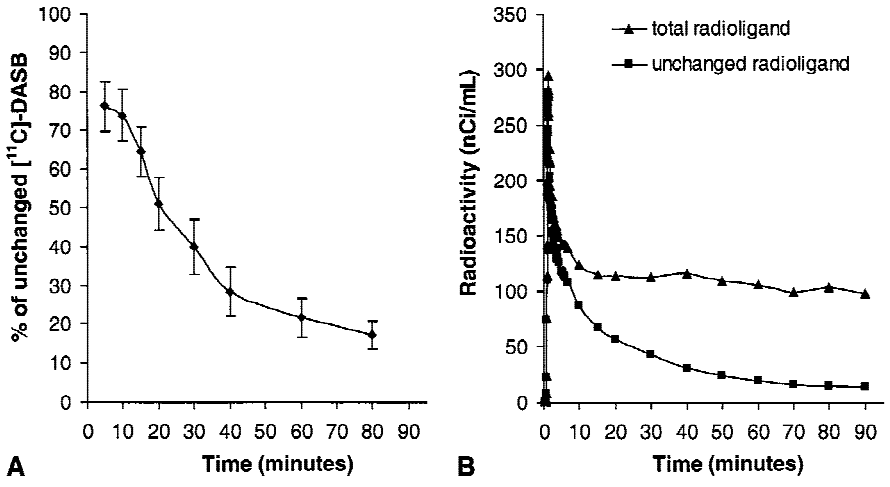

FIG. 2. (A) Time course for the percentage of radioactivity in plasma corresponding to unchanged [^{11}C]-DASB in healthy human subjects (mean ± SD; n = 5). **(B)** Time-activity curves for the concentration of total radioactivity in plasma (triangle) and for the concentration of unchanged radioligand in plasma (square).

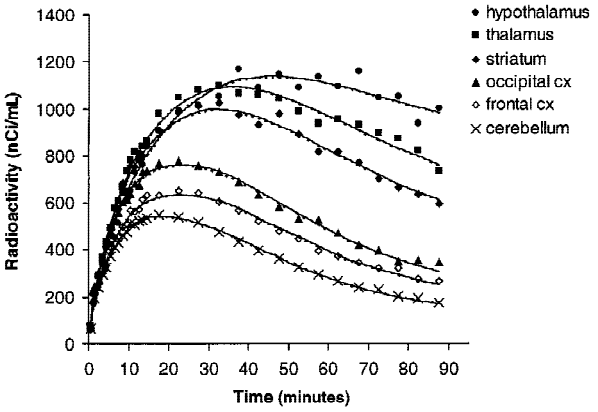

FIG. 3. Representative time-activity curves for regional brain radioactivity obtained after intravenous injection of [11C]-DASB in one healthy subject. For each brain region, the symbols correspond to the experimental measured values, the dashed line corresponds to the fitted curve obtained according to a one-tissue compartment model (Method A), and the solid line corresponds to the fitted curve obtained according to a two-tissue compartment model with K_1/k_2 ratio in target regions of interest fixed to that found in cerebellum with a one-tissue compartment model (Method C).

target ROIs to the DV′ estimated in the cerebellum was sufficient to reach convergence. However, even then, the individual rate constants k_3 and k_4 were estimated with poor precision, as exhibited by the large standard errors in parameters estimates (COV > 100%). Even though individual parameter values for k_3 and k_4 were highly variable, the ratio k_3/k_4 was stable and was estimated with a much higher accuracy. Interindividual variability in k_3/k_4 values were highly consistent across brain regions as assessed by %VAR ranging from 7% in the frontal cortex and striatum to 18% in the occipital cortex (Table 3). As expected, the ratio k_3/k_4, which is proportional to B_{max} (Eq. 4), correlated well with the known regional densities of SERT sites. Comparisons between the mean regional BP values as measured in the current experimental conditions using [11C]-DASB and Method C and the mean [3H]paroxetine specific binding values reported postmortem in corresponding regions of the human brain are shown in Fig. 4. Positron emission tomography measures of [11C]-DASB BP were significantly correlated with the *in vitro* measures of [3H]paroxetine binding sites densities reported by Bäckström et al. (1989) (Fig. 4A; $r^2 = 0.96$; Student's *t*-test: $P < 0.01$) and Laruelle et al. (1988) (Fig. 4B; $r^2 = 0.81$; Student's *t*-test: $P < 0.05$).

Examples of curve fits obtained by applying Methods A and C to [11C]-DASB TAC data are shown in Fig. 3. Goodness of fits was not statistically improved by using Method C as compared with Method A as assessed with F test. In addition, both the AIC (AIC = 88 ± 31 and 90 ± 31 for Method A and C, respectively; repeated measures analysis of variance [ANOVA]: $F_{1,29} = 0.44$; $P > 0.05$) and the SC (SC = 91 ± 31 and 94 ± 31 for Method A and Method C, respectively; repeated measures ANOVA: $F_{1,29} = 1.31$; $P > 0.05$) were not statistically different between the methods.

Method D yielded kinetic parameter estimates that were similar to those obtained with Method C (Table 3). The standard errors on the determination of K_1 values (as demonstrated by %COV) were significantly greater than with Method C (repeated measures ANOVA: $F_{1,29} = 4.64$; $P < 0.05$), which were in turn greater than with Method A (repeated measures ANOVA: $F_{1,29} = 27.76$; $P < 0.001$). Coupling K_1/k_2 between regions during the fitting procedure did not improve the identifiability of k_3 and k_4 with %COV exceeding 100%, but gave k_3/k_4 values that were similar to those obtained with Method C.

In Method F, coupling both K_1/k_2 and k_4 during the fitting procedure significantly improved the identification of [11C]-DASB kinetic parameters. As compared with Methods C and D, Method F significantly decreased the standard errors associated with k_3 and k_4, with %COV ranging from 20% to 30% (Table 3). k_3 values were high and varied between regions according to their relative density of SERT sites. The ratios k_3/k_4 estimated with Method F were identical to those estimated with Method C. Method F did not improve the AIC and SC values as compared with Method C (AIC = 90 ± 31 and 90 ± 31 for Methods C and F, respectively; repeated measures ANOVA: $F_{1,29} = 0.96$; $P > 0.05$; SC = 94 ± 31 and 94 ± 31 for Methods C and F, respectively; repeated measures ANOVA: $F_{1,29} = 0.96$; $P > 0.05$).

TABLE 2. *Rate constants obtained by the kinetic 1CM analysis of [11C]-DASB binding*

Method	Region	K_1 (mL g^{-1} min^{-1})	K_1 COV (%)	k_2' (min^{-1})	k_2' COV (%)	DV′ (mL g^{-1})
A	Cerebellum	0.64 ± 0.11	2.09 ± 0.65	0.053 ± 0.003	2.83 ± 0.84	11.88 ± 1.52
	Striatum	0.70 ± 0.10	1.81 ± 0.16	0.022 ± 0.002	3.25 ± 0.35	32.10 ± 3.73
	Thalamus	0.79 ± 0.13	1.79 ± 0.14	0.022 ± 0.004	3.17 ± 0.37	35.49 ± 4.50
	Hypothalamus	0.62 ± 0.11	1.88 ± 0.17	0.013 ± 0.001	4.64 ± 0.45	47.05 ± 4.66
	Occipital cx.	0.72 ± 0.12	1.80 ± 0.14	0.040 ± 0.004	2.55 ± 0.15	17.97 ± 2.46
	Frontal cx.	0.63 ± 0.12	1.80 ± 0.14	0.040 ± 0.004	2.54 ± 0.14	15.55 ± 2.02

Values are mean ± SD of five experiments. Coefficient of variation (COV) corresponds to the standard error of parameter as given by the diagonal of the covariance matrix during the nonlinear least squares fitting procedure and is expressed as percentage of the parameter value. 1CM, one-tissue compartment model; DV, distribution volume.

TABLE 3. *Rate constants obtained by the kinetic 2CM analysis of [^{11}C]-DASB binding*

Method	Region	K_1 (mL g^{-1} min^{-1})	K_1 COV (%)	K_1/k_2 (mL g^{-1})	K_1/k_2 COV (%)	k_3 (min^{-1})	k_3 COV (%)	k_4 (min^{-1})	k_4 COV (%)	k_3/k_4
C	Cerebellum	0.63 ± 0.10	3.2 ± 0.8	11.88	fixed	0.00 ± 0.00	>100	5.99 ± 2.04	>100	0.00 ± 0.00
	Striatum	0.71 ± 0.11	2.6 ± 0.7	11.88	fixed	2.91 ± 2.33	60.7 ± 50.9	1.76 ± 1.48	47.9 ± 48.9	1.71 ± 0.12
	Thalamus	0.81 ± 0.14	6.2 ± 3.9	11.88	fixed	2.08 ± 1.77	>100	1.02 ± 0.87	>100	2.00 ± 0.34
	Hypothalamus	0.64 ± 0.13	6.6 ± 4.4	11.88	fixed	1.36 ± 0.86	>100	0.44 ± 0.23	>100	2.99 ± 0.40
	Occipital cx.	0.73 ± 0.12	2.9 ± 0.7	11.88	fixed	1.27 ± 1.38	63.7 ± 70.2	2.26 ± 2.17	34.7 ± 34.7	0.51 ± 0.09
	Frontal cx	0.64 ± 0.12	4.0 ± 1.3	11.88	fixed	0.77 ± 0.82	>100	2.33 ± 2.39	29.6 ± 19.4	0.31 ± 0.02
D	Cerebellum	0.63 ± 0.10	2.7 ± 1.0	11.88 ± 1.59	8.5 ± 5.3	0.02 ± 0.04	>100	5.36 ± 2.32	>100	0.00 ± 0.01
	Striatum	0.72 ± 0.13	6.2 ± 7.3	11.88 ± 1.59	8.5 ± 5.3	1.91 ± 1.50	>100	1.17 ± 1.03	>100	1.71 ± 0.13
	Thalamus	0.81 ± 0.14	7.5 ± 5.7	11.88 ± 1.59	8.5 ± 5.3	2.32 ± 2.28	>100	1.14 ± 1.12	>100	2.01 ± 0.34
	Hypothalamus	0.65 ± 0.12	18.1 ± 14.4	11.88 ± 1.59	8.5 ± 5.3	2.27 ± 3.24	>100	0.80 ± 1.18	>100	3.02 ± 0.43
	Occipital cx.	0.74 ± 0.12	5.5 ± 5.7	11.88 ± 1.59	8.5 ± 5.3	0.52 ± 0.67	>100	0.95 ± 1.09	>100	0.52 ± 0.10
	Frontal cx	0.64 ± 0.11	4.4 ± 3.6	11.88 ± 1.59	8.5 ± 5.3	0.37 ± 0.17	>100	1.16 ± 1.08	>100	0.31 ± 0.03
F	Cerebellum	0.63 ± 0.10	2.3 ± 0.8	11.86 ± 1.60	2.6 ± 3.1	0.00 ± 0.00	>100	0.53 ± 0.11	20.4 ± 8.6	0.00 ± 0.01
	Striatum	0.72 ± 0.10	2.1 ± 0.3	11.86 ± 1.60	2.6 ± 3.1	0.92 ± 0.21	23.3 ± 8.1	0.53 ± 0.11	20.4 ± 8.6	1.72 ± 0.12
	Thalamus	0.81 ± 0.14	2.6 ± 0.9	11.86 ± 1.60	2.6 ± 3.1	1.05 ± 0.14	23.1 ± 8.6	0.53 ± 0.11	20.4 ± 8.6	2.01 ± 0.35
	Hypothalamus	0.63 ± 0.11	2.3 ± 0.4	11.86 ± 1.60	2.6 ± 3.1	1.59 ± 0.28	21.8 ± 8.9	0.53 ± 0.11	20.4 ± 8.6	3.00 ± 0.44
	Occipital cx.	0.74 ± 0.13	2.0 ± 0.3	11.86 ± 1.60	2.6 ± 3.1	0.27 ± 0.05	25.2 ± 9.7	0.53 ± 0.11	20.4 ± 8.6	0.52 ± 0.10
	Frontal cx	0.64 ± 0.12	2.0 ± 0.3	11.86 ± 1.60	2.6 ± 3.1	0.17 ± 0.03	27.9 ± 12.4	0.53 ± 0.11	20.4 ± 8.6	0.31 ± 0.03

Values are mean ± SD of five experiments. Coefficient of variation (COV) corresponds to the standard error of parameter estimated by the nonlinear least squares fitting procedure, is expressed in percent of the parameter value and is given as an index of the parameter identifiability. 2CM, two-tissue compartment model.

Stability of k_3/k_4 values versus study duration

To define the minimum PET data acquisition time required to derive stable BP values using method C, all regional time-activity curves were fitted for various periods of time ranging from 40 minutes to 90 minutes in 10-minute increments (Fig. 5). k_3/k_4 values for less than 70-minute study duration were greater than for 90 minutes, especially in regions with high density of SERT sites such as hypothalamus. With only 40 minutes of data included, k_3/k_4 increased to 130% of the 90-minute value. In regions with lower density of SERT sites, stable values for BP were reached for study duration greater than 50 minutes. Similar results were obtained for derivation of DV′ (data not shown). In the 2 subjects tested, extending PET scanning time to 120 minutes yielded outcome measures that were close (within 5%) to their 90-minute value.

Simplified method analyses

Total distribution volume values derived from the Logan graphical approach produced comparable results to those obtained using the kinetic 1CM approach (Table 4). The 2 measures were significantly correlated (slope = 0.87; r^2 = 0.98; Student's *t*-test: $P < 0.001$). However, the graphical approach yielded DV values that were significantly less (range: −3% to −19%; mean: −8%) than those estimated with the 1CM approach (Table 4; repeated measures ANOVA: $F_{1,29} = 6.18$; $P < 0.02$). Underestimation of total DV using the graphical approach was more pronounced in regions with high SERT levels such as hypothalamus.

The average BP values obtained by the five different methods are given in Table 5. Binding potential values obtained by the four simplified methods were in close agreement with those obtained by the kinetic Method C. The interindividual variability was greater for the ratio method and smallest for the transient equilibrium method. The peak of specific binding uptake was reached between 40 and 50 minutes in the cortical regions, and between 50 and 60 minutes in the striatum and thalamus. In the hypothalamus, time for transient equilibrium oc-

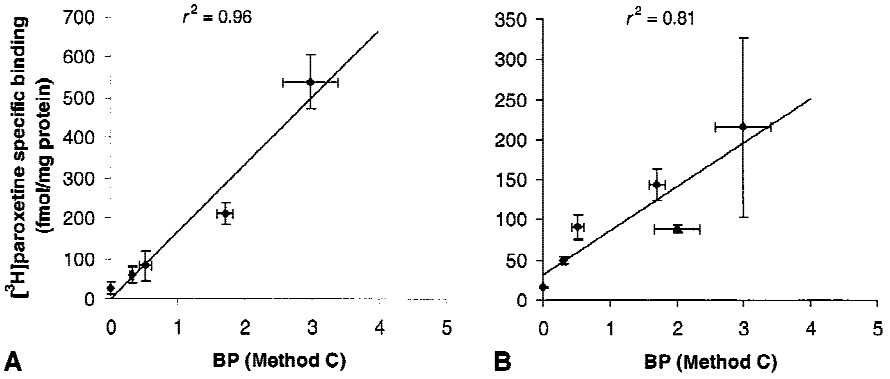

FIG. 4. Correlations between [^{11}C]-DASB binding potential (BP) values in various brain regions as determined using Method C and the density of [^{3}H]paroxetine binding sites reported by **(A)** Bäckström et al. (1989) and **(B)** Laruelle et al. (1988).

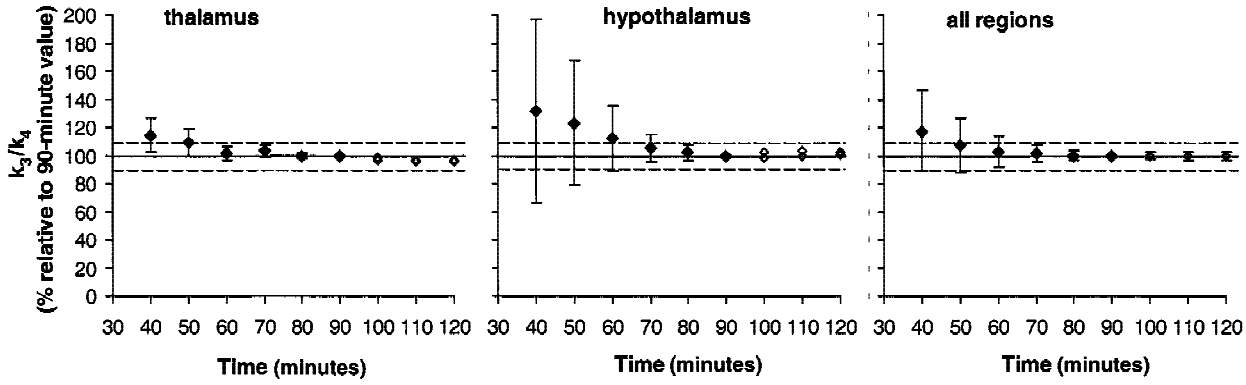

FIG. 5. Effect of study duration on the stability of k_3/k_4 ratio values as estimated with Method C in the thalamus, hypothalamus, and all regions combined. For less than 90 minutes of study duration (closed symbols), each parameter was expressed as the mean ± SD (n = 5) percentage of the value obtained when 90 minutes of acquisition data was considered. In 2 of the 5 subjects examined, positron emission tomography data acquisition time was extended to 120 minutes. The parameter values obtained at extended times and expressed as percentage of the relative 90-minute value obtained in each subject is also plotted (open symbols).

curred later and was not reached within the time frame of the experiment (90 minutes) in 3 of the 5 subjects. Hence, the transient equilibrium approach was not always applicable in the hypothalamus.

The BP calculated with the graphic, the SRTM, and the ratio methods were compared with the BP obtained with Method C. The error in BP calculated with the graphic method (range: −9% to +3%; mean: −5%) were smaller than those calculated with the SRTM method (range: −9% to +20%; mean: −7%), which in turn were smaller than those calculated with the ratio method (range: −13% to +26%; mean: +14%).

Simulations

Errors in BP_{ratio} for assumed k_3/k_4 and K_1 values are shown in Fig. 6. Decreases in K_1 were associated with underestimation of BP_{ratio}, whereas increases in K_1 were associated with overestimation of BP_{ratio}. For all k_3/k_4 values, increases in K_1 values up to 30% led to errors in the estimation of BP_{ratio} that were less than 10%. Underestimation in BP_{ratio} greater than 10% were observed for K_1 values less than 20% and k_3/k_4 values greater than 2. The effect of changes in K_1 on BP_{SRTM} was small with maximal error inferior to 1% (data not shown).

TABLE 4. *Comparison of total distribution volume values between methods*

Region	Method A		Graphic	
	DV′	% VAR	DV_{Logan}	% VAR
Cerebellum	11.9 ± 1.5	13	11.2 ± 1.3	12
Striatum	32.1 ± 3.7	12	29.9 ± 3.6	12
Thalamus	35.5 ± 4.9	13	33.0 ± 3.8	12
Hypothalamus	47.0 ± 4.7	10	41.1 ± 6.4	15
Occipital cx.	18.0 ± 2.5	14	16.9 ± 2.0	12
Frontal cx.	15.6 ± 2.0	13	14.6 ± 1.7	12

Values are mean ± SD of five experiments. %VAR corresponds to the intersubject variability in the paramater estimates. DV, distribution volume.

DISCUSSION

The primary goal of this study was to evaluate methods to obtain reliable estimates of SERT density from the analysis of [^{11}C]-DASB brain uptake curves in humans. As previously described (Houle et al., 2000), the regional distribution of [^{11}C]-DASB uptake was concordant with the known densities of SERT sites in the brain. The highest levels of radioactivity were observed in the hypothalamus, intermediate levels were observed in the thalamus and striatum, whereas modest to low levels of radioactivity were observed in the cortical regions and cerebellum, respectively.

Kinetic analyses of [^{11}C]-DASB brain uptake curves revealed that a 1CM was sufficient to describe the time-activity data. Convergence was achieved in all subjects and all brain regions. The transport parameter K_1 was high, indicating that [^{11}C]-DASB is highly extracted, and was estimated precisely in all regions. The moderate intersubject variability of 10% to 14% suggested that the 1CM does provide sufficiently accurate estimates of [^{11}C]-DASB total distribution volumes, DV′. Although DV′ includes information both on radioligand delivery and binding to specific receptor sites, at equilibrium DV′ should be independent of tracer delivery and is assumed to give an index of receptor site density. This assumption was supported by the observation that the rank order of DV′ values correlated well with the typical rank order of SERT densities found in the human brain postmortem (Cortes et al., 1988; Laruelle et al., 1988; Backstrom et al., 1989).

The free and nonspecific distribution volume measured for [^{11}C]-DASB in the cerebellum was high (DV′ = 11.9 ± 1.5 mL g^{-1}) as compared with that of other neuroreceptor radioligands—such as the D_2-receptor antagonist [^{11}C]raclopride (0.42 ± 0.06 mL g^{-1}; Lammerstma et al., 1996), the $5HT\text{-}_{1A}$ receptor antagonist [carbonyl-^{11}C]WAY-100635 (0.54 ± 0.11 mL g^{-1}; Gunn

TABLE 5. *Comparison of BP values obtained using different methods*

Region	Method C		Simplified methods							
	BP	VAR (%)	BP_{Logan}	VAR (%)	BP_{SRTM}	VAR (%)	BP_{ratio}	VAR (%)	BP_{Eq}	VAR (%)
Cerebellum	0.00 ± 0.00	—	NA		NA		NA		NA	
Striatum	1.71 ± 0.12	7	1.67 ± 0.13	8	1.62 ± 0.16	10	1.79 ± 0.22	12	1.64 ± 0.12	7
Thalamus	2.00 ± 0.34	17	1.96 ± 0.33	17	1.91 ± 0.31	16	2.09 ± 0.43	21	1.86 ± 0.30	16
Hypothalamus	2.99 ± 0.40	13	2.68 ± 0.47	18	2.68 ± 0.68	25	2.49 ± 0.64	26	2.89 ± 0.34*	12*
Occipital cx.	0.51 ± 0.09	18	0.51 ± 0.10	19	0.51 ± 0.11	20	0.59 ± 0.14	24	0.48 ± 0.08	16
Frontal cx.	0.31 ± 0.02	7	0.30 ± 0.03	9	0.31 ± 0.04	12	0.37 ± 0.05	15	0.31 ± 0.02	7

Values are mean ± SD of five experiments. *In the hypothalamus, transient equilibrium was not identifiable in all subjects and BP_{Eq} was calculated in only three out of five subjects. %VAR corresponds to the intersubject variability in the parameter estimates. BP, binding potential.

et al., 1998), or the D_1-receptor antagonist [^{11}C]NNC 112 (2.54 ± 0.42 mL g^{-1}; Abi-Dargham et al., 2000). [^{11}C]-DASB DV′ measured in cerebellum is likely to represent an appropriate estimate of the nondisplaceable DV. Indeed, several postmortem studies in humans reported either undetectable (Cortes et al., 1988) or extremely low SERT site density (Backstrom et al., 1989; Laruelle et al., 1988) in the cerebellum. Furthermore, Western blot analysis disclosed only a trace amount of SERT protein in autopsied human cerebellar cortex (S. Kish, personal communication). Such high values for free and nonspecific DV seems to be a property shared by several SERT radioligands. Indeed, cerebellar distribution volume values equal to 17.8 ± 1.9 mL g^{-1} and 16.8 ± 4.0 mL g^{-1} have been reported for [^{11}C]-McN 5652 in humans (Parsey et al., 2000) and [^{11}C]venlafaxine in swine (Smith et al., 1997), respectively.

An unconstrained 2CM with the estimation of four kinetic parameters failed to reach convergence in all subjects and all brain regions. Reducing the complexity of the 2CM by reducing the number of floating parameters solved the convergence problem. This was done by different methods that all constrained parameter values in the model that were predicted not to have large variations between brain regions. Method C consisted to estimate the free and nonspecific binding from the cerebellum, a region relatively devoid of SERT sites, and to subsequently use that estimate in the analysis of receptor-rich region kinetics. This approach has been used successfully to improve the kinetic parameter estimation of several radioligands such as [^{11}C]flumazenil (Price et al., 1993), [^{123}I]iomazenil (Laruelle et al., 1994), or [^{11}C]MDL 100,907 (Watabe et al., 2000). Method C did not allow identification of k_3 and k_4 individually, but was found to provide reasonably precise estimates of the ratio between the two rate constants k_3/k_4. The difficulty in deriving reliable individual estimates of k_3 and k_4 from a 2CM three parameters configuration while obtaining a relatively stable ratio between both parameters has already been reported by Koeppe et al. (1991) for kinetic analysis of [^{11}C]flumazenil. This problem with parameter identifiability is because of the rapid equilibration occurring between the free and nonspecific and the specifically bound ligand compartments that preclude their kinetic identification with accuracy. The rapid rate of [^{11}C]flumazenil binding as compared with its brain delivery rate has led Koeppe et al. (1991) to propose a 1CM kinetic analysis for [^{11}C]flumazenil. This simplified configuration also appears to be the method of choice for [^{11}C]-DASB. Moreover, a strong overall correlation across the 5 subjects was observed ($r = 0.96$) between k_3/k_4 (BP) values estimated from Method C and the DV′ values estimated from the 1CM, indicating that DV′ is an appropriate parameter for assessing [^{11}C]-DASB binding site density.

A limitation of the aforementioned kinetic approaches is that both assume that the use of cerebellum as a reference region to estimate free and nonspecific binding is valid. Although postmortem studies did not reveal significant levels of [^{3}H]paroxetine binding in human cerebellum (Cortes et al., 1988; Laruelle et al., 1988; Backström et al., 1989), a 2CM analysis with a more precise identification of receptor-related parameters in cerebel-

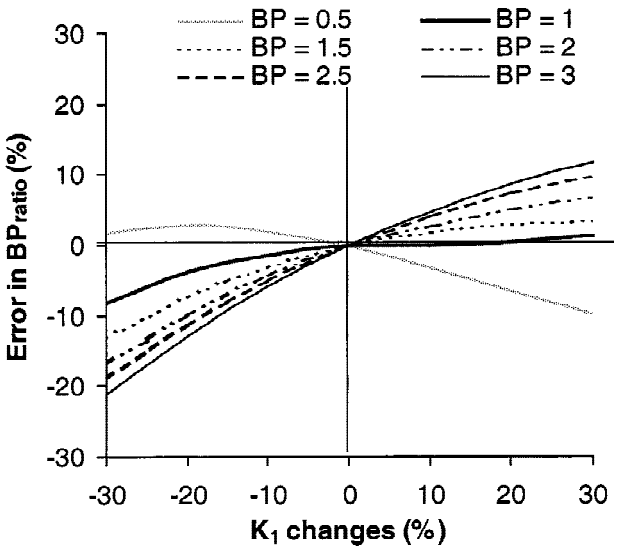

FIG. 6. Errors caused by changes in k_3/k_4 and K_1 values on binding potential (BP) values calculated using the ratio method.

lum would further validate this assumption. In an attempt to improve the identifiability of k_3 and k_4, a second set of methods (Methods D, E, and F) was evaluated that consisted to couple every set of ROI data with a common parameter or a combination of common parameters during the 2CM fitting procedure. These methods have the advantage that no reference region is required to estimate the free and nonspecific binding. Fitting simultaneously data from all regions while coupling parameters that are supposed to be similar across regions increase the amount of data available. This fitting strategy has been shown to substantially increase the identifiability of kinetic parameters (Raylman et al., 1994; Buck et al., 1996, 2000). Because both the free and nonspecific binding and the molecular dissociation constant k_4 are expected to be similar across regions, the authors fit their data by coupling either one of these parameters or both.

Coupling both the free and nonspecific binding and k_4 substantially reduced the COVs on k_3 and k_4 estimates, and enabled the 2CM fitting procedure to determine the relative contribution of free and nonspecific and specific pools with acceptable levels of accuracy. k_3 values, which are directly related to B_{max}, were extremely low in cerebellum, further supporting its use as a reference region for analysis of [^{11}C]-DASB PET experiments.

The ratios k_3/k_4, which equal B_{max}/K_D, ranged from 0.31 in the frontal cortex to 2.99 in the hypothalamus with intermediate values of 2.00 in the thalamus. From a conceptual point of view, the ratio k_3/k_4, as determined in the current study, is similar to the equilibrium specific to nonspecific partition coefficient values noted for V_3'' and used by certain authors to evaluate B_{max}/K_D. V_3'' values previously reported for [^{11}C](+)-McN 5652 in humans are close to 0 in several regions of the frontal cortex and are equal 0.92 and 1.63 in thalamus and hypothalamus, respectively (Parsey et al., 2000). The higher SERT density indices obtained with [^{11}C]-DASB as compared with those obtained with [^{11}C](+)-McN 5652 favor [^{11}C]-DASB as a more suitable radioligand for *in vivo* evaluation of the SERT.

Scan duration is a factor to consider when evaluating a prospective new PET radioligand for clinical evaluation in patients. Indeed, the scan duration needs to be long enough to obtain stable estimates of receptor-related parameters but, at the same time, it has to be short enough both to meet patient compliance and to avoid excessive distortion of the time-activity data by incremental noise. The latter is especially important late in the study because of decay of the short half-life carbon 11 radionucleotide. These criteria were fulfilled with [^{11}C]-DASB because the authors determined that no longer than 80 minutes of data acquisition were needed to provide stable measures of both DV′ and k_3/k_4 values in all brain regions.

The transient equilibrium, the graphical analysis, the ratio, and the STRM methods gave BP values in good agreement with those obtained with the kinetic Method C. Distribution volume values derived by the graphical and the kinetic (Method A) approaches were strongly correlated, but the graphical approach yielded systematic lower values. Underestimation of DV values derived from the Logan graphical analysis has already been described and has been demonstrated to be caused by the sensitivity of this approach to statistical noise (Abi-Dargham et al., 2000). However, the advantage of estimating DV with the graphical approach is that no assumption is required concerning the rate of equilibration between compartments. When compared with the BP obtained with the kinetic approach, the graphical and the transient equilibrium approaches yielded the smallest errors in BP estimates (5% average underestimation for both methods). However, the need for arterial sampling and plasma metabolite analysis in the graphical approach and the inapplicability of the transient equilibrium approach in SERT-rich regions when 90 minutes of PET data are considered preclude their use for derivation of BP values in routine clinical studies.

The SRTM method slightly underestimated BP (by an average of 7%), whereas large overestimations of BP (by an average of 14%) were obtained when using the ratio method. The ratio method used late time-activity data that are not obtained under equilibrium conditions and that have been demonstrated to be more affected by statistical noise (Lammertsma et al., 1996; Ito et al., 1998). This can explain at least in part the larger errors obtained with this method. Moreover, the simulation study indicated that the errors introduced by decreases in regional CBF in target brain regions relative to the reference region on the determination of BP_{ratio} were larger than 10% in SERT-rich regions. The authors concluded that the SRTM method is the most suitable method for routine quantification of SERT density indexes using PET and [^{11}C]-DASB, because it estimates BP values with reasonable bias, it does not require determination of an arterial input function, and this method, as theoretically predicted, is not sensitive to potential differences in CBF between the target and the reference regions.

In summary, [^{11}C]-DASB can be used to visualize and quantify SERT density in the human brain. The distribution of radiotracer accumulation is consistent with the known densities of SERT sites. The 1CM was more applicable than the standard 2CM, as the latter exhibited problems with model convergence. A constrained 2CM with estimation of 3 kinetic parameters did not improve goodness of fits as compared with the 1CM, but did provide stable BP estimates that were significantly correlated with the density of SERT sites reported *in vitro*. Thus, calculation of the BP from a 2CM (3 parameters) or an estimation of DV′ from the simplified 1CM are the

2 alternatives for estimation of SERT densities using [^{11}C]-DASB. Simplified quantitative methods based on the use of cerebellum as a reference region gave BP values in good agreement with those obtained using the kinetic approach. Among the four simplified methods evaluated, the SRTM method was chosen as the most suitable because it gave the best trade-off between lowest errors in BP estimates, easy applicability for routine use, and lowest sensitivity to potential changes in regional CBF.

The suitability of [^{11}C]-DASB for quantitative examination of the SERT *in vivo* using PET is thus supported by the observations that tissue data can be described using a kinetic analysis and that simplified quantitative methods, using the cerebellum as a reference region, provide reliable estimates of SERT binding parameters.

Acknowledgments: The authors gratefully acknowledge Kevin Cheung for assistance during the PET experiments, Verdell Goulding for the subject's recruiting, and Armando Garcia, Jin Li, and Ruiping Guo for radiochemistry support.

REFERENCES

Abi-Dargham A, Martinez D, Mawlawi O, et al (2000) Measurement of striatal and extrastriatal dopamine D1 receptor binding potential with [^{11}C]NNC 112 in humans: validation and reproducibility. *J Cereb Blood Flow Metab* 20:225–243

Acton PD, Kung MP, Mu M, et al (1999) Single-photon emission tomography imaging of serotonin transporters in the non-human primate brain with the selective radioligand [^{123}I]IDAM. *Eur J Nucl Med* 26:854–861

Akaike H (1974) A new look at the statistical model identification. *IEEE Trans Automat Contr* 19:716–723

Bäckström I, Bergström M, Marcusson J (1989) High affinity [^{3}H] paroxetine binding to serotonin uptake sites in human brain tissue. *Brain Res* 486:261–268

Buck A, Westera G, vonSchulthess GK, Burger C (1996) Modeling alternatives for cerebral carbon-11-iomazenil kinetics. *J Nucl Med* 37:699–705

Buck A, Gucker PM, Schonbachler RD, et al (2000) Evaluation of serotonergic transporters using PET and [^{11}C](+)McN-5652: assessment of methods. *J Cereb Blood Flow Metab* 20:253–262

Burger C, Buck A (1997) Requirements and implementation of a flexible kinetic modeling tool. *J Nucl Med* 38:1818–1823

Carson RE (1986) Parameters estimation in positron emission tomography. In: *Positron emission tomography. Principles applications for the brain and the heart* (Phelps ME, Mazziota JC, Schelbert HR, eds), New York: Raven Press, pp 347–390

Carson RE, Channing MA, Blasberg RG, et al (1993) Comparison of bolus and infusion methods for receptor quantitation: application to [^{18}F]cyclofoxy and positron emission tomography. *J Cereb Blood Flow Metab* 13:24–42

Cash R, Raisman R, Ploska A, Agid Y (1985) High and low affinity [^{3}H]imipramine binding sites in control and parkinsonian brains. *Eur J Pharmacol* 117:71–80

Choi SR, Hou C, Oya S, et al (2000) Selective *in vitro* and *in vivo* binding of [^{125}I]ADAM to serotonin transporters in rat brain. *Synapse* 38:403–412

Cortes R, Soriano E, Pazos A, et al (1988) Autoradiography of antidepressant binding sites in the human brain: localization using [^{3}H]Imipramine and [^{3}H]Paroxetine. *Neuroscience* 27:473–496

Crow TJ, Cross AJ, Cooper SJ, et al (1984) Neurotransmitter receptors and monoamine metabolites in the brains of patients with Alzheimer-type dementia and depression, and suicides. *Neuropharmacol* 23:1561–1569

Farde L, Eriksson L, Blomquist G, Halldin C (1989) Kinetic analysis of central [^{11}C]raclopride binding to D_2-dopamine receptors studied by PET: a comparison to the equilibrium analysis *J Cereb Blood Flow Metab* 9:696–708

Gunn RN, Sargent PA, Bench CJ, et al (1998) Tracer kinetic modeling of the 5-HT1A receptor ligand [carbonyl-^{11}C]WAY-100635 for PET. *Neuroimage* 8:426–440

Hashimoto K, Inoue O, Suzuki K, et al (1987) Synthesis and evaluation of [^{11}C]cyanoimipramine. *Int J Rad Appl Instrum B* 14:587–592

Houle S, Ginovart N, Hussey D, et al (2000) Imaging the serotonin transporter with positron emission tomography: initial human studies with [^{11}C]DAPP and [^{11}C]DASB. *Eur J Nucl Med* 27:1719–1722

Hume SP, Lammertsma AA, Bench CJ, et al (1992) Evaluation of S-[^{11}C]citalopram as a radioligand for *in vivo* labelling of 5-hydroxytryptamine uptake sites. *Int J Rad Appl Instrum B* 19:851–855

Ito H, Hietala J, Blomqvist G, et al (1998) Comparison of the transient equilibrium and continuous infusion method for quantitative PET analysis of [^{11}C]raclopride binding. *J Cereb Blood Flow Metab* 18:941–950

Koeppe RA, Holthoff VA, Frey KA, et al (1991) Compartmental analysis of [^{11}C]flumazenil and kinetics for the estimation of ligand transport rate and receptor distribution using positron emission tomography. *J Cereb Blood Flow Metab* 11:735–744

Kung M P, Hou C, Oya S, et al (1999) Characterization of [^{123}I]IDAM as a novel single-photon emission tomography tracer for serotonin transporters. *Eur J Nucl Med* 26:844–853

Lammertsma AA, Hume SP (1996) Simplified reference tissue model for PET receptor studies. *Neuroimage* 4:153–158

Lammertsma AA, Bench CJ, Hume SP, et al (1996) Comparison of methods for analysis of clinical [^{11}C]raclopride studies. *J Cereb Blood Flow Metab* 16:42–52

Laruelle M, Vanisberg MA, Maloteaux JM (1988) Regional and subcellular localization in human brain of [^{3}H]paroxetine binding, a marker of serotonin uptake sites. *Biol Psych* 24:299–309

Laruelle M, Baldwin RM, Rattner Z, et al (1994) SPECT quantification of [^{123}I]iomazenil binding to benzodiazepine receptors in nonhuman primates: I. Kinetic modeling of single bolus experiments. *J Cereb Blood Flow Metab* 14:439–452

Lasne MC, Pike VW, Turton DR (1989) The radiosynthesis of [N-methyl-^{11}C]-sertraline. *Int J Rad Appl Instrum [A]* 40:147–151

Leenders KL, Perani D, Lammerstma AA, et al (1990) Cerebral blood flow, blood volume and oxygen utilization. Normal values and effect of age. *Brain* 113:27–47

Litton JE, Holte S, Eriksson L (1990) Evaluation of the Karolinska new positron camera: the Scanditronix PC2048–15B. *IEEE Trans Nucl Sci NS* 37:743–748

Logan J, Fowler JS, Volkow ND, et al (1990) Graphical analysis of reversible radioligand binding from time-activity measurements applied to [N-^{11}C-methyl]-(-)-Cocaine PET studies in human subjects. *J Cereb Blood Flow Metab* 10:740–747

Marquardt DW (1963) An algorithm for least-squares estimation on non-linear parameters. *J Soc Ind Appl Math* 11:431–441

Maryanoff BE, Vaught JL, Shank RP, et al (1990) Pyrroloisoquinoline antidepressants. 3. A focus on serotonin. *J Med Chem* 33:2793–2797

Mikolajczyk K, Szabatin M, Rudnicki P, et al (1998) A JAVA environment for medical image analysis: initial application for brain PET quantification. *Med Inf* 23:207–214

Mintun MA, Raichle ME, Kilbourn MR, et al (1984) A quantitative model for the *in vivo* assessment of drug binding sites with positron emission tomography. *Ann Neurol* 15:217–227

Oya S, Kung MP, Acton PD, et al (1999) A new single-photon emission computed tomography imaging agent for serotonin transporters: [^{123}I]IDAM, 5-iodo-2-((2-((dimethylamino)methyl)phenyl)-thio)benzyl alcohol. *J Med Chem* 42:333–335

Oya S, Choi SR, Hou C, et al (2000) 2-((2-((dimethylamino)methyl)-phenyl)thio)-5-iodophenylamine (ADAM): an improved serotonin transporter ligand. *Nucl Med Biol* 27:249–254

Parsey RV, Kegeles LS, Hwang DR, et al (2000) In vivo quantification of brain serotonin transporters in humans using [^{11}C]McN 5652. *J Nucl Med* 41:1465–1477

Price JC, Mayberg HS, Dannals RF, et al (1993) Measurement of benzodiazepine receptor number and affinity in humans using tracer kinetic modeling, positron emission tomography, and [^{11}C]Flumazenil. *J Cereb Blood Flow Metab* 13:656–667

Raylman RR, Hutchins GD, Beanlands RS, Schwaiger M (1994) Modeling of carbon-11-acetate kinetics by simultaneously fitting data from multiple ROIs coupled by common parameters. *J Nucl Med* 35:1286–1291

Schwartz G (1978) Estimating the dimension of a model. *Ann Statist* 6:461–464

Shiue CY, Shiue GG, Cornish KG, O'Rourke MF (1995) PET study of the distribution of [^{11}C]fluoxetine in a monkey brain. *Nucl Med Biol* 22:613–616

Smith DF, Jensen PN, Gee AD, et al (1997) PET neuroimaging with [^{11}C]venlafaxine: serotonin uptake inhibition, biodistribution and binding in living pig brain. *Eur Neuropsychopharmacol* 7:195—200

Stanley M, Virgilio J, Gershon S (1982) Tritiated imipramine binding sites are decreased in the frontal cortex of suicides. *Science* 216:1337–1339

Studholme C, Hill DLG, Hawkes DJ (1997) Automated three-dimensional registration of magnetic resonance and positron emission tomography brain images by multiresolution optimisation of voxel similarity measures. *Med Phys* 24:25–35

Suehiro M, Wilson AA, Scheffel U, et al (1991) Radiosynthesis and evaluation of N-(3-[^{18}F]fluoropropyl)paroxetine as a radiotracer for *in vivo* labeling of serotonin uptake sites by PET. *Int J Radiat Appl Instrum B* 18:791–796

Szabo Z, Scheffel U, Suehiro M, et al (1995) Positron emission tomography of 5-HT transporter sites in the baboon brain with [^{11}C]McN5652. *J Cereb Blood Flow Metab* 15:798–805

Watabe H, Channing MA, Der MG, et al (2000) Kinetic analysis of the 5-HT$_{2A}$ ligand [^{11}C]MDL 100,907. *J Cereb Blood Flow Metab* 20:899–909

Wilson AA, Houle S (1999) Radiosynthesis of carbon-11 labelled N-Methyl-2-(arylthio)benzylamines: potential radiotracers for the serotonin reuptake receptor. *J Labelled Compd Radiopharm* 42:1277–1278

Wilson AA, Ginovart N, Schmidt M, et al (2000*a*) Novel radiotracers for imaging the serotonin transporter by positron emission tomography: synthesis, radiosynthesis, and *in vitro* and ex vivo evaluation of [^{11}C]-labeled 2-(phenylthio)araalkylamines. *J Med Chem* 43:3103–3110

Wilson AA, Garcia A, Jin L, Houle S (2000*b*) Radiotracer synthesis from [^{11}C]-iodomethane: a remarkably simple captive solvent method. *Nucl Med Biol* 27:529–532